Human Molecular Genetics, 2008, Vol. 17, No. 2 **201–214**
doi:10.1093/hmg/ddm297
Advance Access published on October 9 2007

LETM1, deleted in Wolf–Hirschhorn syndrome is required for normal mitochondrial morphology and cellular viability

Kai Stefan Dimmer[1], Francesca Navoni[1], Alberto Casarin[2], Eva Trevisson[2], Sabine Endele[3], Andreas Winterpacht[3], Leonardo Salviati[2] and Luca Scorrano[1,*]

[1]Dulbecco-Telethon Institute, Venetian Institute of Molecular Medicine, 35129 Padova, Italy, [2]Section of Human Genetics, Department of Paediatrics, University of Padova, 35121 Padova, Italy and [3]Institute of Human Genetics, University Hospital Erlangen, Friedrich-Alexander-University, 91054 Erlangen, Germany

Received August 22, 2007; Revised and Accepted October 7, 2007

Wolf–Hirschhorn syndrome (WHS) is a complex congenital syndrome caused by a monoallelic deletion of the short arm of chromosome 4. Seizures in WHS have been associated with deletion of *LETM1* gene. *LETM1* encodes for the human homologue of yeast Mdm38p, a mitochondria-shaping protein of unclear function. Here we show that human LETM1 is located in the inner membrane, exposed to the matrix and oligomerized in higher molecular weight complexes of unknown composition. Down-regulation of *LETM1* did not disrupt these complexes, but led to DRP1-independent fragmentation of the mitochondrial network. Fragmentation was not associated with changes in the levels of respiratory chain complexes, or with obvious or latent mitochondrial dysfunction, but was recovered by nigericin, which catalyzes the electroneutral exchange of K^+ against H^+. Down-regulation of *LETM1* caused 'necrosis-like' death, without activation of caspases and not inhibited by overexpression of Bcl-2. Primary fibroblasts from a WHS patient displayed reduced *LETM1* mRNA and protein, but mitochondrial morphology was surprisingly unaffected, raising the question of whether and how WHS patients counteract the consequences of monoallelic deletion of *LETM1*. *LETM1* highlights the relationship between mitochondrial ion homeostasis, integrity of the mitochondrial network and cell viability.

INTRODUCTION

Wolf–Hirschhorn syndrome (WHS; OMIM 194190) has an incidence of 1/50 000 and is characterized by severe growth retardation, loss of muscular tone, mental retardation, hypertelorism, microcephaly, dysgenic corpus callosum, speech problems and epilepsy. Seizures characterize the full WHS phenotype: they start during the first year of life and are a frequent cause of death (1). WHS is caused by the partial deletion of the short arm of one chromosome 4 involving chromosome region 4p16.3 (2). WHS is thought to be a contiguous gene deletion syndrome with an unknown number of genes contributing to the phenotype. A WHS critical region (WHSCR-1) has been defined to a 165 kb region encompassing several genes (3,4). The variety of combination of symptoms and the different severity in different patients reflects the diverse extents of the chromosomal deletion in individual patients. Seizures constitute the most life-threatening problem in WHS and have been initially associated with deletion of the $GABA_A$ receptor gene, which however maps proximal to the critical deletion region (WHSCR), specifically, 4p12–p13 (5). Recently, a novel gene, *LETM1*, <80 kb distal to the WHSCR-1, was cloned (6). *LETM1* has been found to lie within the newly proposed critical region WHSCR-2, and to be invariably associated with a complete clinical picture, including seizures (2). The idea that LETM1 could play a role in seizures of WHS patients was also substantiated by the finding that it possessed two putative Ca^{2+} binding EF hands (6), and that it was a mitochondrial protein (7), like its homologue in *Saccharomyces cerevisiae*, Mdm38p.

*To whom correspondence should be addressed at: Istituto Veneto di Medicina Molecolare, Via Orus 2, 35129 Padova, Italy. Tel: +39 0497923221; Fax: +39 0497923271; Email: lscorrano@dti.telethon.it

Mitochondria are crucial organelles for life and death of the cell. They produce most of the ATP, participate in Ca^{2+} signalling and integrate diverse apoptotic stimuli by releasing protein cofactors needed in the cytosol for activation of effector caspases (8,9). Mitochondrial shape changes, i.e. fission of the mitochondrial reticulum and cristae remodelling, are crucial to ensure apoptosis progression (10–13). Mitochondria recently attracted interest as players in the pathogenesis of seizures: mtDNA mutations result in mitochondrial dysfunction and seizures (14) and apoptosis follows seizures in the newborn (15). In this respect, haploinsufficiency of *LETM1* could be a central event in the pathogenesis of seizures associated to WHS.

Mdm38p, the yeast homologue of *LETM1*, was discovered in a genome-wide screening to be involved in the maintenance of mitochondrial morphology (16). Lack of Mdm38p leads to disruption of the subcortical mitochondrial network and apparent swelling of mitochondria. The molecular function of this protein is poorly understood. It has been suggested that Mdm38p is involved in mitochondrial K^+ homeostasis, by regulating, or by physically being a component of the long sought mitochondrial K^+/H^+ antiporter (17). Loss of the master regulator of mitochondrial K^+ homeostasis would cause an increase in mitochondrial K^+ levels, leading to an influx of water into the matrix that could explain the 'swollen' mitochondrial phenotype (18). Alternatively, Mdm38p has also been proposed to be involved in the export of proteins to the inner membrane and in the biogenesis of complexes III and IV. Mdm38p shares functional homology with the well-characterized Oxa1-complex, that is responsible for the insertion of mitochondrially encoded proteins. Mdm38p binds mitochondrial ribosomes and when this interaction is disrupted by its ablation, assembly and therefore steady-state levels of amounts of electron chain complexes were altered (19).

Function of *LETM1* is even less understood. It has been recently reported that ablation of *Letm1* in *Caenorhabditis elegans* is lethal at larval stage, while RNA interference (RNAi)-mediated down-regulation of its expression results in increased mortality. The mechanism by which this is exerted is unclear. In mammalian mitochondria, LETM1 is found in high molecular weight (MW) fractions, consistent with its tendency to homointeract. Its ablation causes derangement of mitochondrial morphology, with a 'swollen' appearance, similar to what is observed in yeast and in *C. elegans* (20). Taken together, these results suggest that LETM1 could participate in the regulation of mitochondrial volume. Nevertheless, they raise several questions: is the mitochondrial fragmentation caused by ablation of LETM1 direct, or is it orchestrated by the Drp1-dependent fission machinery? Do levels of LETM1 control mitochondrial respiratory chain complexes and function of the organelle? And finally, what is the consequence of LETM1 ablation on viability?

In order to address these questions and to gain insights into the function of LETM1, we studied the biochemical properties of LETM1 and the effects of its ablation on mitochondrial physiology, morphology and cellular viability. Our results indicate that LETM1 is located in the inner mitochondrial membrane, with the bulk of the protein facing the matrix, in a high MW oligomer. Ablation of LETM1 causes Drp1 independent mitochondrial fragmentation, while levels of the respiratory chain complexes, mitochondrial respiratory rates and membrane potential are unaffected. The changes in mitochondrial morphology can be pharmacologically reverted by the nigericin, which catalyzes the K^+/H^+ exchange across biological membranes. Unexpectedly, mitochondrial fragmentation by LETM1 results in caspase-independent, necrotic death. Taken together, our results suggest that LETM1 is a regulator of mitochondrial shape independently of the classical Drp1-dependent pathway, and its ablation results in loss of viability.

RESULTS

Subcellular and submitochondrial localization of LETM1

In silico analysis of the sequence of LETM1 does not provide information on the putative function of the protein, but gives clues on its cellular localization. LETM1 is conserved throughout eukaryotic organisms, and a classical mitochondrial presequence is predicted in LETM1, like in its homologue in yeast Mdm38p. Furthermore, LETM1 possesses, close to its N-terminus, a hydrophobic stretch long enough to span a membrane. Interestingly, this predicted transmembrane domain contains three conserved proline residues. Proteins which are imported and inserted into the inner mitochondrial membrane follow two distinct routes (21): they are laterally inserted into the membrane by the TIM23-complex, or they pursue the classical import pathway into the matrix and re-enter the inner membrane from inside mitochondria. Proline residues in the transmembrane domain are indicative of the latter and therefore suggest that the main C-terminal part of LETM1 is located in the matrix. We therefore examined the distribution of LETM1 in subcellular and submitochondrial fractions in HeLa cells. LETM1 was located only in a mitochondrial fraction, like the bona fide mitochondrial markers Tom20 and Opa1, and not in the microsomal and cytosolic fractions (Fig. 1A). Carbonate extraction experiment showed that LETM1 is an integral membrane protein (Fig. 1B). In order to verify the submitochondrial localization of this integral membrane protein, we performed a subfractionation of mitochondria followed by separation of individual compartments on a Percoll gradient. Albeit the outer mitochondrial membrane fraction was contaminated by a small amount of inner membrane, LETM1 was found in the inner mitochondrial membrane fraction and in smaller amount in the matrix (Fig. 1C). This could represent a slight contamination of the matrix fraction with components of the inner membrane, or it could suggest that LETM1 transits from the matrix before being inserted in the inner membrane. In order to understand orientation of LETM1 in the inner membrane, we turned to a protease accessibility assay. LETM1 was protected from cleavage by proteinase K (PK) as long as the inner membrane remained intact. This reactivity was shared by matrix proteins, like mitochondrial Hsp70; conversely, inner membrane proteins exposed to the intermembrane space (IMS), like Opa1, were readily digested when the outer face of the inner membrane was exposed to the protease by osmotically swelling mitochondria (Fig. 1D). In conclusion, our data suggest that C-terminal bulk of LETM1 is

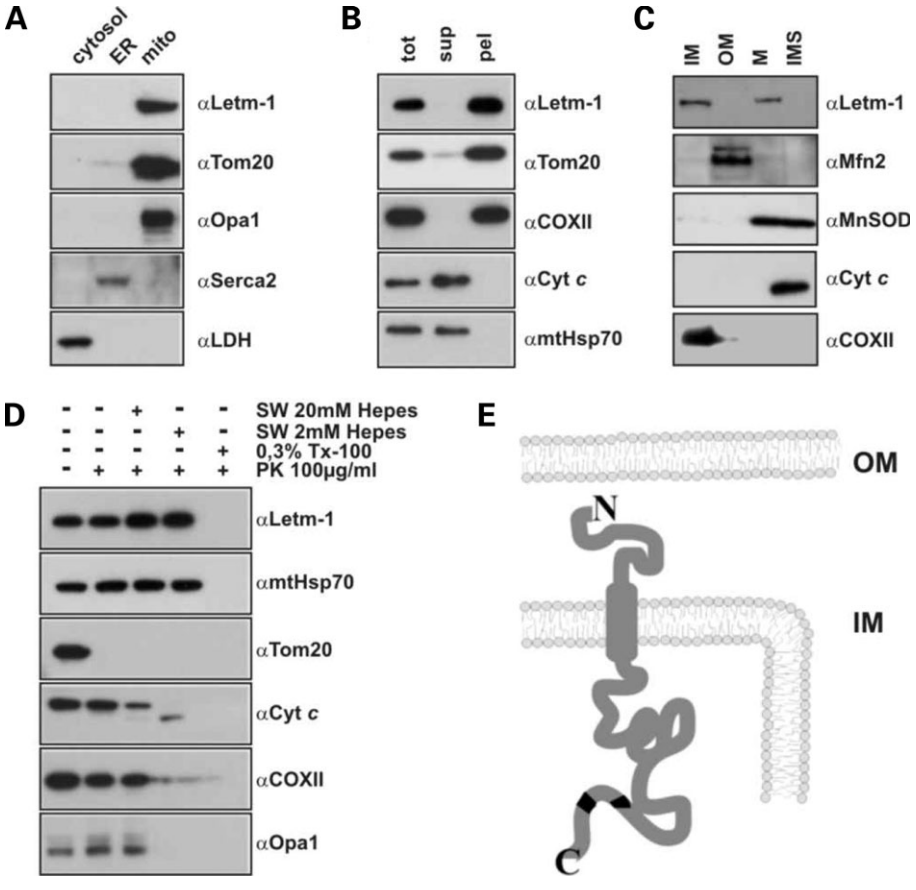

Figure 1. LETM1 is an inner mitochondrial membrane protein facing the matrix. (**A**) Subcellular fractions of HeLa cells were prepared and 10 μg of protein of each fraction was separated by SDS–PAGE and immunoblotted using the indicated antibodies. (**B**) Carbonate extraction. Purified mitochondria were incubated in 0.1 M Na_2CO_3 pH 11 for 30 min at 4°C. Soluble and membrane fractions were separated by centrifugation for 1 h, 4°C, 24 000*g* and equal amounts (10 μg) of proteins were separated by SDS–PAGE and immunoblotted using the indicated antibodies. (**C**) Submitochondrial fractionation was performed as described in material and methods and equal amounts (25 μg) of proteins from inner membrane (IM), outer membrane (OM), matrix (M) and intermembrane space (IMS) were separated by SDS–PAGE and immunoblotted using the indicated antibodies. Note that the LETM1 immunoreactive band in the matrix runs at a slightly higher molecular weight (MW) than the one in the inner membrane. (**D**) Proteinase K accessibility assay. Purified mitochondria (0.1 mg/ml) incubated in isolation buffer were treated as indicated in the figure and 10 μg of protein was separated by SDS–PAGE and immunoblotted using the indicated antibodies. SW, swelling. (**E**) Cartoon depicting the mitochondrial localization of LETM1.

likely to be protected from protease cleavage by the inner membrane, while cleavage of the small N-terminus is not detectable by size shift in SDS–PAGE. Thus, LETM1 likely is an integral inner membrane protein that faces the matrix (Fig. 1E).

LETM1 oligomerizes in higher MW complexes

The prototypical Na^+/H^+ antiporter possesses 12 alpha helices, while prediction of secondary structure of LETM1 indicated the existence of only one putative transmembrane domain. This structure is not suggestive of a direct role of LETM1 in ion exchange. Nevertheless, we decided to explore the possibility that in native conditions LETM1 assembles in higher MW complexes, which in principle could represent a suitable site for ion exchange across the inner membrane. To this end, we wished to analyze the organization of LETM1. First, we explored whether crosslinking of HeLa mitochondria with an amino-specific (disuccinimidyl suberate, DSS) or a thiol-specific (beta maleimido hexane, BMH) reagent yielded higher MW adducts, immunoreactive for LETM1. In BMH-treated mitochondria, two adducts which could correspond to a dimer (∼140 kDa) and a trimer (∼210 kDa) of LETM1 (∼70 kDa) were visible, while in the case of DSS we only observed the ∼210 kDa adduct (Fig. 2A). We further investigated LETM1 organization by blue native gel electrophoresis to confirm the higher MW LETM1 containing complexes suggested by crosslinking and to determine their size. Di-dodecyl maltoside (DDM) solubilized mitochondria showed three major higher MW complexes immunoreactive for LETM1, with an apparent size of ∼250, 500 and 650 kDa. Interestingly, the distribution of LETM1 in these complexes depended on the concentration of DDM: increasing DDM concentration led to a decreased LETM1 immunoreactivity in the 650 kDa complex, in favour of the 500 kDa one (Fig. 2B). Second dimension denaturing SDS–PAGE of the DDM solubilized complexes identified a smeared immunoreactivity for LETM1 in a MW range comprised between ∼220 and 850 kDa (Fig. 2D). In order to verify specificity of the complexes, we decided to monitor

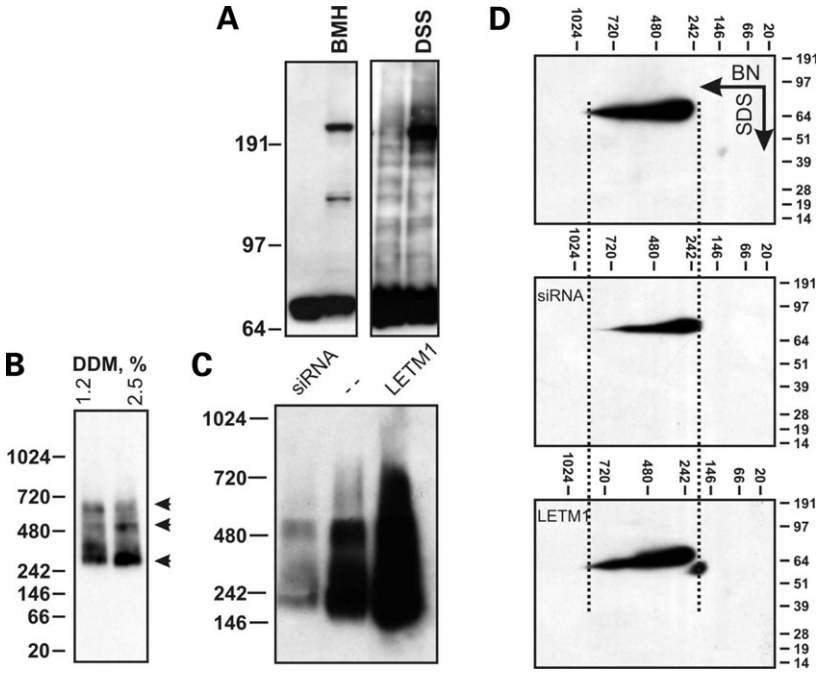

Figure 2. LETM1 is organized in higher MW complexes in the inner mitochondrial membrane. (**A**) Purified mitochondria were treated where indicated with 0.5 mM DSS or 0.5 mM BMH for 30 min, followed by centrifugation and TCA precipitation. Thirty μg of proteins in the pellets were separated by SDS–PAGE and immunoblotted using anti-LETM1 antibodies. (**B**) Purified HeLa mitochondria were incubated for 30 min at 4°C with the indicated concentrations (w/V) of DDM and 50 μg of proteins were separated by BN-PAGE and immunoblotted using anti-LETM1 antibodies. (**C**) HeLa cells were transfected with a scrambled siRNA (- -), with LETM1-specific siRNA (siRNA), or with pcDNA3.1-Letm1 (Letm1). After 24 h, mitochondria were isolated and solubilized using 2.5% DDM. BN-PAGE and immunoblotting was performed as in (B) (**D**) Experiment was performed as in (C). Following isolation of the complexes by BN-PAGE, lanes were excised and mounted on a second dimension SDS–PAGE as described in Materials and Methods. Proteins were separated and immunoblotted using an anti-LETM1 antibody.

them in mitochondria from cells where *LETM1* expression had been silenced by RNAi or where *LETM1* was overexpressed. In both cases, the three prominent LETM1 immunoreactive complexes were readily identifiable, suggesting that the existence of these complexes did not depend critically on the levels of LETM1. The second dimension analysis further confirmed this possibility and showed a lower MW LETM1-immunoreactive band accumulated outside from the LETM1-containing complexes in LETM1-overexpressing complexes (Fig. 2C and D). The appearance of this band, likely a degradation product, was also evident from immunoblotting of mitochondrial proteins from LETM1-overexpressing mitochondria separated by conventional SDS–PAGE (Fig. 3A). Taken together, these data indicate that LETM1 is part of at least three inner mitochondrial protein complexes of unknown composition. Moreover, they indicate that these complexes are maintained in mitochondria where *LETM1* is silenced or overexpressed, suggesting that levels of LETM1 are not essential for the correct assembly of the complexes. Finally, overexpression of LETM1 results in its degradation to a lower MW species by an unknown protease.

Levels of LETM1 regulate mitochondrial morphology

We next wished to verify whether mitochondrial morphology was affected by changes in the levels of LETM1. Following specific RNAi, LETM1 was efficiently reduced (Fig. 3A) to ~40% in comparison to cells transfected with a scrambled RNA, as determined by densitometry on five different experiments (not shown). When we analyzed mitochondrial morphology, we found that silencing of *LETM1* resulted in large, dot-like mitochondria that clustered in the perinuclear region (Fig. 3B and quantification in C). This phenotype was also observed in other cells such as the human osteosarcoma U2OS cell line (not shown). The pictures of mitochondria lacking LETM1 were reminiscent of what observed following overexpression of pro-fission proteins such as Fis1 (22) or ablation of pro-fusion ones like Opa1 (23). In both cases, inhibition of the Drp1-dependent fission machinery, by silencing or by using a dominant negative, $Drp1^{K38A}$ mutant recovers mitochondrial morphology (24,25). We therefore sought to determine whether the phenotype induced by down-regulation of *LETM1* was similarly complemented by ablation or inhibition of Drp1. Co-transfection of HeLa cells with siRNAs directed against *LETM1* and *Drp1* efficiently reduced expression of both proteins (Fig. 3D). In HeLa cells that normally show already elongated mitochondria, silencing of *Drp1* resulted in further elongation of the mitochondrial tubules (arrowhead in Fig. 3E). Nevertheless, co-silencing of *Drp1* did not recover the fragmented phenotype induced by reduction of LETM1 (Fig. 3E and quantification in F). Similarly, silencing of *LETM1* in cells expressing $DRP1^{K38A}$ resulted in mitochondrial fragmentation (Fig. 3F). Thus, adequate levels of LETM1 are essential to maintain mitochondrial morphology and blockage of the fission machinery does not recover the fragmented phenotype induced by silencing of

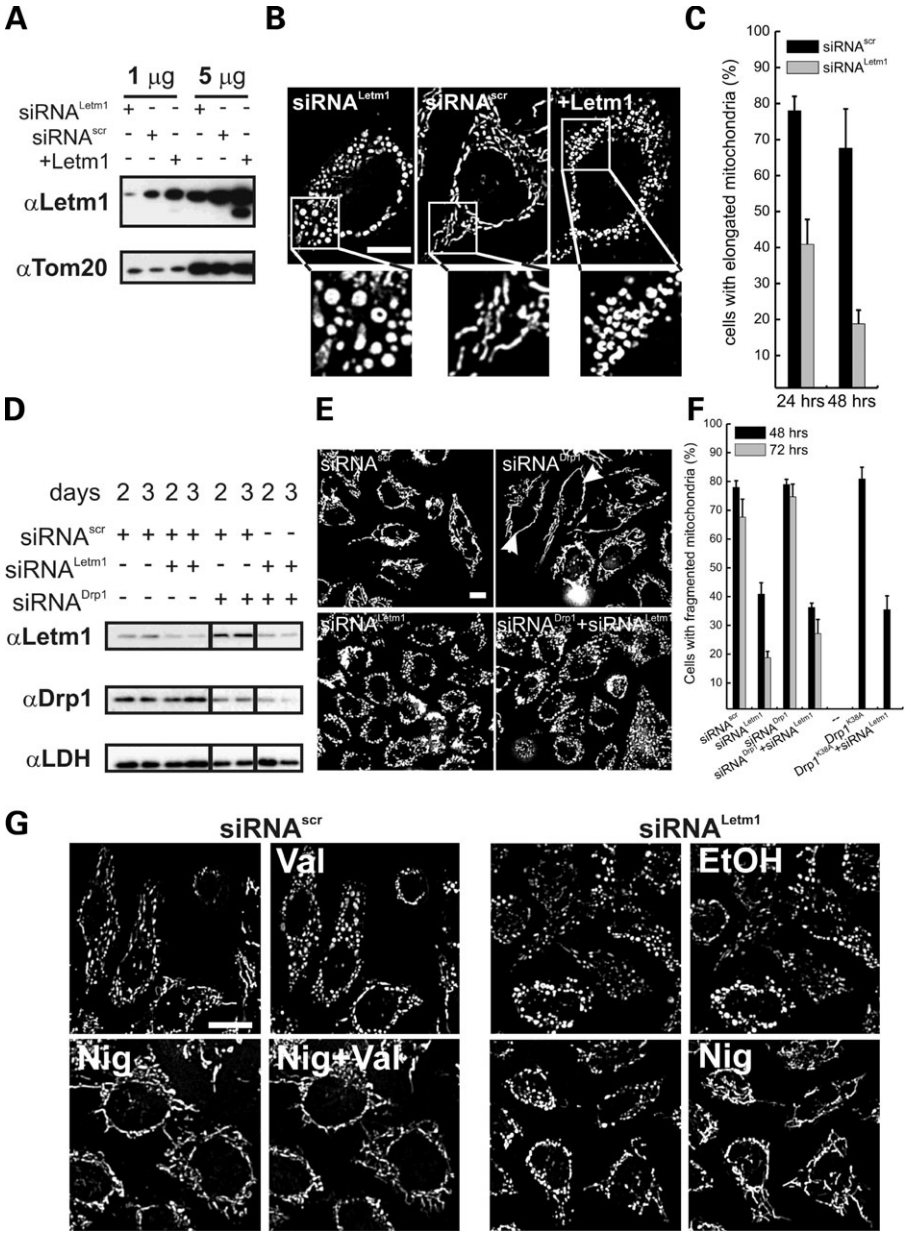

Figure 3. Lack of LETM1 causes Drp1-independent mitochondrial fragmentation. (**A**) HeLa cells were transfected with the indicated siRNA or with pcDNA3.1-Letm1 (+Letm1) and after 48 h mitochondria were isolated, lysed and the indicated amount of protein was separated by SDS–PAGE and immunobloted using the indicated antibodies. (**B**) Representative epifluorescence images of mitochondrial morphology. HeLa cells stably expressing mtRFP were transfected with the indicated siRNA; alternatively, HeLa cells were cotransfected with mtRFP and *LETM1* and after 48 h images were acquired and deconvolved as described. Bar, 10 μm. Boxed areas are enlarged 2.7×. (**C**) Quantitative analysis of mitochondrial shape changes. Experiments were performed as in (B) and morphometric analysis was performed in blind as described in Materials and Methods. Data represent mean ± SE of three independent experiments ($n > 400$ cells each condition). (**D**) HeLa cells were transfected with the indicated siRNA and after the indicated time lysed and the indicated amount of protein was separated by SDS–PAGE and immunobloted using the indicated antibodies. Black lines show irrelevant lanes that were eliminated from the picture of the blot. (**E**) Representative epifluorescence images of mitochondrial morphology. HeLa cells stably expressing mtRFP were transfected with the indicated siRNA and after 48 h images were acquired and deconvolved as described. Bar, 10 μm. Arrowheads point to cells with highly elongated mitochondria. (**F**) Quantitative analysis of mitochondrial shape changes. Experiments were performed as in (E) and morphometric analysis was performed in blind as described in Materials and Methods. Data represent mean ± SE of three independent experiments. In the right part of the graph, HeLa cells were cotransfected with mtRFP and the indicated siRNA and/or plasmid. After 24 h, mitochondrial morphology was evaluated as described in (E). Data represent mean ± SE of four independent experiments. (**G**) Nigericin restores mitochondrial morphology following down-regulation of *LETM1*. HeLa cells stably expressing mtRFP were transfected with the indicated siRNA and after 48 h images were acquired and deconvolved as described. Where indicated, cells were treated for 20 min with 2 μM nigericin (Nig), for 15 min with 1 μM valinomycin (Val) or for 20 min with 0.1%, V/V vehicle (EtOH). Bar, 20 μm. Images are representative frames from at least three independent real time mitochondrial morphology imaging experiments.

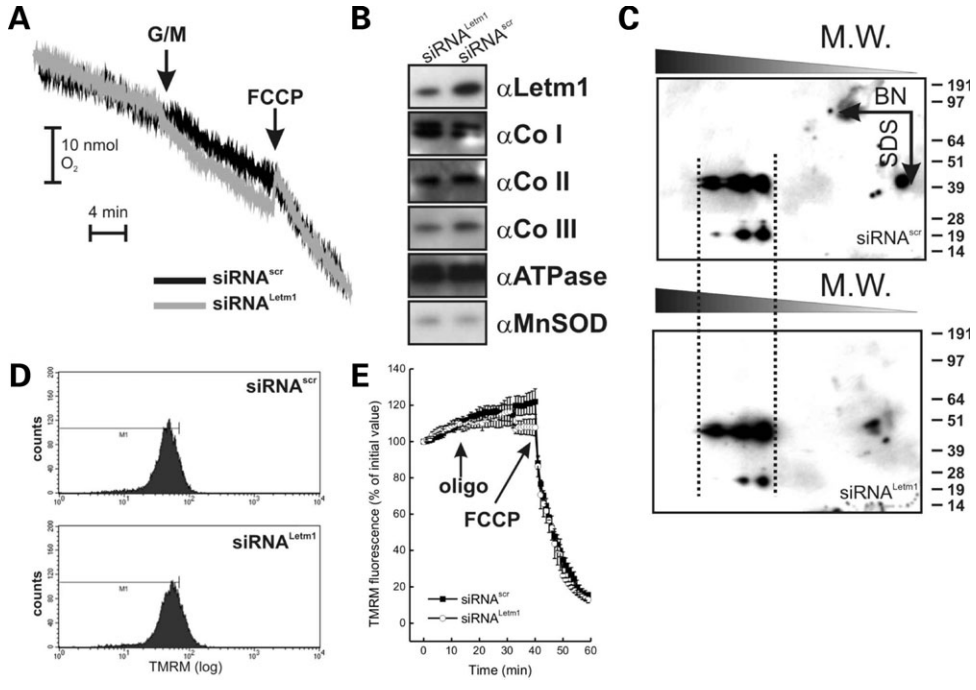

Figure 4. Effect of *LETM1* silencing on biogenesis of mitochondrial respiratory chain complexes and mitochondrial function. (**A**) Representative traces of respiration of mitochondria of the indicated genotype. HeLa cells were transfected with the indicated siRNA and after 48 h mitochondria were isolated and transferred into an oxygen electrode chamber containing experimental buffer (125 mM KCl, 10 mM Tris-MOPS, 10 μM EGTA-Tris, 1 mM Pi). Where indicated (arrows), 5 mM glutamate/2.5 mM malate (G/M) and 60 nM FCCP were added. (**B**) Levels of nuclear-encoded components of individual respiratory chain complexes. HeLa cells were transfected with the indicated siRNA and after 48 h mitochondria were isolated, lysed and equal amounts (10 μg) of proteins were separated by SDS–PAGE and immunoblotted using the indicated antibodies raised against the OXPHOS complexes. (**C**) Two-D, BN-, SDS–PAGE of mitochondria isolated from HeLa cells transfected with the indicated siRNA were performed as described in Figure 2D and immunoblotted using an anti-complex III antibody. (**D**) Flow cytometric analysis of TMRM uptake. HeLa cells transfected with the indicated siRNA after 48 h were stained with TMRM and uptake was determined by flow cytometry as described in Materials and Methods. (**E**) Quantitative analysis of TMRM fluorescence changes over mitochondrial regions in HeLa cells transfected as indicated. Twenty-four hours after transfection, cells. Data represent mean ± SE of five independent experiments. Where indicated (arrows), 1 μM oligomycin and 2 μM FCCP were added.

LETM1. This prompted us to address whether fragmentation could be counteracted by restoration of K^+/H^+ antiport by pharmacological means. To this end, we took advantage of the antibiotic nigericin, a well-characterized monocarboxylate polyether that catalyzes the exchange of one K^+ ion with one H^+ across biological membranes, including mitochondria (26) and that has been successfully employed to revert the mitochondrial phenotype of the Δ*mdm31* and *32 S. cerevisiae* strain (27). Pretreatment with nigericin counteracted mitochondrial fragmentation induced by the K^+ ionophore valinomycin and restored shape of the mitochondrial network in HeLa cells where *LETM1* was down-regulated by siRNA (Fig. 3G). In conclusion, these experiments point out to a relationship between LETM1, K^+ homeostasis and mitochondrial morphology.

Upon overexpression of *LETM1*, mitochondria also appeared fragmented, often organized in round, doughnut-like structures, smaller than the species observed following silencing of the protein (Fig. 3D). This morphology is often a sign of mitochondrial distress and is for example observed in cells treated with the ATPase inhibitor oligomycin, or with the uncoupler FCCP (not shown). Given that overexpression of *LETM1* results in the appearance of LETM1 band with faster mobility (probably caused by unspecific proteolysis, Figs 2D and 3A), we interpreted this morphology as an unspecific mitochondrial response to protein overload.

Silencing of *LETM1* does not impair mitochondrial function

Since mitochondrial fragmentation caused by the silencing of *LETM1* was not complemented by blockage of the fission pathway, we reasoned that it could represent the visual counterpart of an underlying mitochondrial dysfunction. This would furthermore be in agreement with both proposed functions of its yeast orthologue Mdm38p in K^+/H^+ antiport, or insertion of proteins into the inner membrane. We therefore decided to explore function of mitochondria lacking LETM1. Silencing of *LETM1* did not affect basal, as well as uncoupled respiration supported by the complex I substrate glutamate (Fig. 4A). In accordance to this, levels of complexes of the respiratory chain, as well as of the ATPase, were unaffected (Fig. 4B). Not only levels, but also assembly of respiratory complexes, like complex III, were unaltered, as indicated by two-dimensional blue native electrophoresis followed by SDS–PAGE (Fig. 4C). These data indicate that silencing of *LETM1* is not sufficient to influence levels of the respiratory chain components and their assembly into complexes. Nevertheless, they do not exclude the possibility that mitochondrial dysfunction occurs *in situ*. To verify this possibility, we measured the cellular uptake of the potentiometric dye tetramethyl rhodamine methyl ester (TMRM), that depends on the plasma and mitochondrial membrane

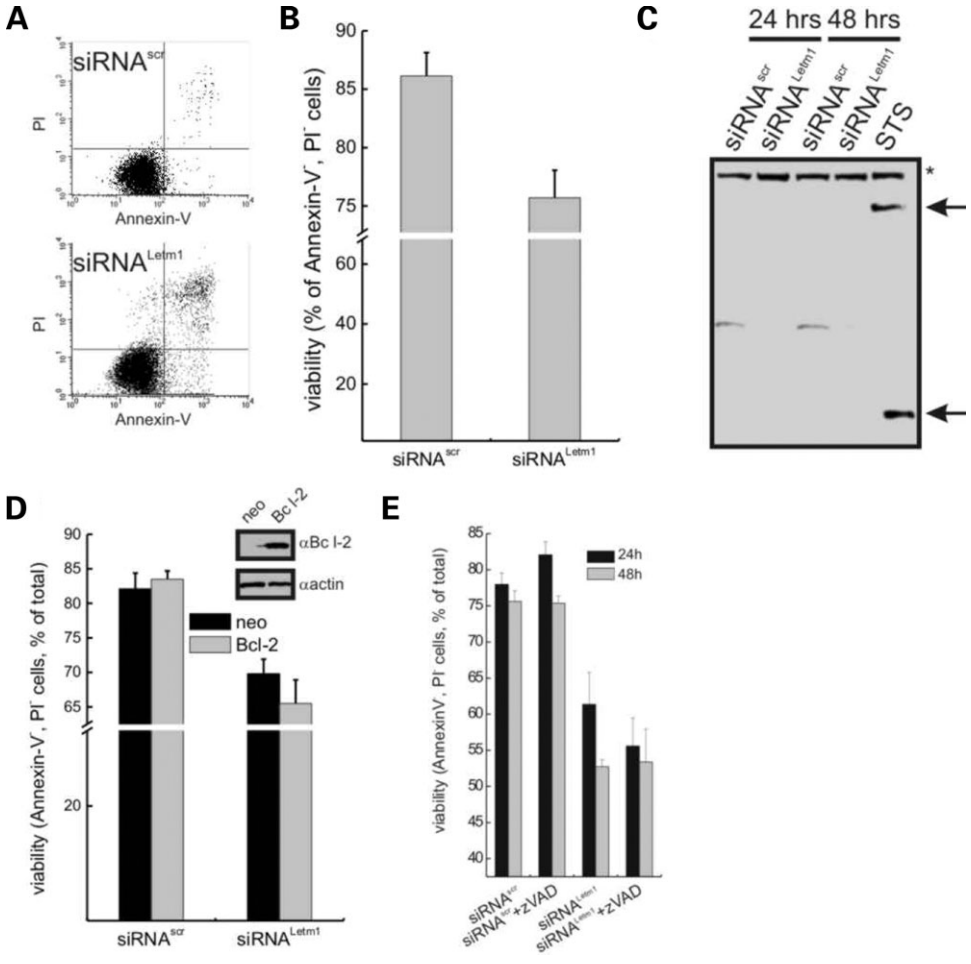

Figure 5. Loss of LETM1 causes caspase-independent, Bcl-2 insensitive cell death. (**A**) Representative dot plots of Annexin-V-FLUOS, PI staining of HeLa cells transfected for 24 h with the indicated siRNA. (**B**) Quantitative analysis of the effect of LETM1 reduction on viability. Experiments were as in (A). Data represent mean ± SE of three independent experiments. (**C**) Silencing of *LETM1* does not result in PARP cleavage. HeLa cells were transfected with the indicated siRNA, and after the indictaed times lysed and equal amounts (50 μg) of protein were separated by SDS–PAGE and immunoblotted with an anti-PARP antibody. Rightmost lane was loaded with 50 μg of proteins from untransfected HeLa cells treated for 12 h with 2 μM staurosporine (STS). Asterisk, uncleaved PARP; arrowheads, caspase cleaved PARP fragments. (**D**) Death caused by silencing of *LETM1* is not blocked by Bcl-2. HeLa cells of the indicated genotype were transfected with the indicated siRNA and after 24 h viability was measured. Inset shows levels of Bcl-2. Equal amounts (50 μg) of protein from cells of the indicated genotype were separated by SDS–PAGE and immunoblotted using the indicated antibodies. (**E**) Death caused by ablation of *LETM1* is not insensitive to inhibition of caspases. HeLa cells were transfected with the indicated siRNA and treated where indicated with 50 μM zVAD-fmk for the whole duration of the experiment. At the indicated times, cells were harvested and viability was determined. Data represent mean ± SE of four independent experiments.

potential. Flow cytometry showed that down-regulation of *LETM1* did not impair uptake of the dye even when cells were pretreated with 50 mM KCl to depolarize the plasma membrane and therefore to drive TMRM uptake only by mitochondrial membrane potential (Fig. 4D). *In situ*, membrane potential of dysfunctional mitochondria can be maintained by the proton pumping activity of the reversal of the ATPase. This latent mitochondrial dysfunction can be unveiled by oligomycin, a specific inhibitor of the ATPase (28). Real time imaging of TMRM fluorescence intensity in mitochondria showed that upon addition of oligomycin, mitochondrial membrane potential increased irrespective of LETM1 levels (Fig. 4E). In conclusion, mitochondrial function measured *in situ* and *in vitro* is unaffected by ablation of ∼60% of LETM1, raising the question of whether the residual LETM1 is sufficient to maintain the mitochondrial functions measured here.

Silencing of *LETM1* causes Bcl-2 insensitive, caspase-independent cell death

In order to understand the functional relevance of the mitochondrial fragmentation caused by silencing of LETM1, we explored if it was associated with changes in viability. Silencing of LETM1 in HeLa cells caused *per se* after 24 h an increase in AnnexinV/propidium iodide (PI) staining, indicative of their reduced viability (Fig. 5A and B). Interestingly, the percentage of single PI-positive cells increased from 2 to 8, suggesting that cells lacking this mitochondrial protein are more prone to necrosis. Furthermore, PARP cleavage, a sign of caspase activation, was undetectable in cells where *LETM1* was silenced, while it was prominent in cells treated with the apoptotic inducer staurosporine (Fig. 5C). We therefore decided to check if death was affected by two different strategies to inhibit apoptosis, at the mitochondrial as well

as at the post-mitochondrial level. We first turned to an HeLa cell line stably overexpressing the mitochondrial antiapoptotic protein Bcl-2 that blocks the release of cytochrome *c* and of other mitochondrial proapoptotic proteins (29). Overexpression of Bcl-2 was completely ineffective in blocking death caused by silencing of *LETM1* (Fig. 5D). Similarly, the addition of the pan-caspase inhibitor z-VAD had no effect whatsoever on the loss of viability induced by the loss of LETM1 (Fig. 5E). Taken together, these results show that silencing of *LETM1* triggers caspase-independent, Bcl-2 insensitive death.

Levels of LETM1 and mitochondrial morphology in cells from patients with severe WHS

In order to explore whether the down-regulation of *LETM1* by siRNA could be a faithful model of WHS, we established a lymphoblastoid cell line from a WHS patient with the full clinical phenotype. This patient suffered from seizures and had a cryptic terminal deletion 4p16.3 sizing 2.2–2.8 Mb, with breakpoint between the deleted cosmid probe LA04NC01-33c6 (MXD4) and the non-deleted cosmid probe LA04NC01-247f6 (SH3BP2) (not shown), encompassing both WHS-critical regions 1 and 2. Deletion of the *LETM1* gene was verified by fluorescence *in situ* hybridization (FISH) with cosmid LA04NC01-75b9, which includes the 5′end of the *LETM1* gene and was caused by the loss of the paternal allele, as shown by a microsatellite marker 182 Kb cetromeric to *LETM1* (Fig. 6B). The generated, transformed lymphoblastoid cell line was then probed for levels of LETM1 protein, which were unexpectedly unchanged (Fig. 6C). To address whether this was a cell-specific effect, possibly related to the transformation of the lymphoblastoid line, we decided to generate a primary fibroblasts from a different patient, also suffering from severe WHS. Real-time PCR analysis of genomic as well as of mRNA *LETM1* showed a clear ∼50% reduction (Fig. 6D). Evaluation of LETM1 by immunoblotting in the same sample revealed a corresponding reduction in the levels of the protein (Fig. 6F and densitometric analysis in E). It should be noted that a repeated analysis of LETM1 in these fibroblasts showed a certain degree of variability. Levels of LETM1 in WHS fibroblasts, assessed by densitometry following normalization for the cytosolic protein LDH, were on average 63.9 ± 12.1% of those detected in the age and sex matched control ($n = 5$, $P = 0.12$ in a two paired Student's *t*-test). Mitochondrial morphology, measured by loading fibroblasts with the potentiometric probe TMRM and assessed as previously described (23), was unexpectedly unaffected in the WHS sample (Fig. 6F and quantification in G).

DISCUSSION

Most of the proteins that regulate shape of mitochondria are associated to the outer mitochondrial membrane. Only a few ones [Opa1/Mgm1p (30,31), or Mdm31p, Mdm32p (32) and Mdm33p (33)] reside inside mitochondria. The control of mitochondrial morphology and dynamics from 'inside' mitochondria is therefore much less understood. Furthermore, although the processes that alter mitochondrial morphology during programmed cell death are well studied, we have scarce knowledge of how mitochondrial morphology is regulated during life of the cell and how this impacts on integrated cellular processes (34,35). In this respect, the yeast protein Mdm38p and its human homologue LETM1 are interesting candidates to integrate regulation 'from the inside' of mitochondrial shape changes to the normal life of the cell. Mdm38p is indeed supposed to be involved in ion homeostasis across (17), or insertion of respiratory chain components into (19), the inner membrane. Furthermore, deletion of *LETM1* is associated with epilepsy in WHS patients (2). Thus, knowledge of the function of LETM1 is not only crucial to clarify how morphology of the mitochondria can be influenced by ions and/or assembly of the respiratory chain complexes, but also to better understand pathogenesis of seizures in WHS.

LETM1, like its yeast homologue, is located in the inner mitochondrial membrane with its bulge C-terminal part facing the matrix. This is consistent with the presence of prolines in the only predicted transmembrane domain of this protein, which are highly suggestive of protein transit from the matrix, followed by re-insertion into the inner membrane (21). Accordingly, in subfractionation experiments of mitochondria we observed traces of LETM1 in the matrix compartment, albeit this could also represent a slight contamination of this subfraction with components of the inner membrane. This latter hypothesis is somehow reinforced by the lack of soluble LETM1 in the carbonate extratction experiment. The topology that we propose is in accordance with what observed for Mdm38p in yeast (17,19) and slightly different from what proposed for LETM1 (20). This discrepancy could be caused by the fact that in the latter experiments by Hasegawa and van der Bliek, digitonin instead of osmotic swelling was used to make IMS accessible to protease. Thus, it is possible that higher concentrations of digitonin caused a certain degree of solubilization of the inner membrane and leaving matrix proteins accessible to the action of protease. In accordance to this hypothesis, in the experiments by Hasegawa and van der Bliek (20) the susceptibility pattern of glutamate dehydrogenase seems to be superimposable to that of LETM1. Furthermore, both functions so far ascribed to LETM1 (participation to K^+ homeostasis or to protein export) are more likely to require a protein whose bulk is exposed to the matrix, rather than a protein facing the IMS. In conclusion, while our experiments favour the orientation of LETM1 proposed in Fig. 1E, the accurate mapping of LETM1 topology requires additional proofs using antibodies against different epitopes of the molecule.

Blue native electrophoresis indicated that once inserted in the inner membrane, LETM1 is retrieved in at least three higher MW complexes, with apparent MW of ∼250, 500 and 650 kDa. Furthermore, crosslinking with the thiol-selective reagent BMH identified an additional complex at ∼140 kDa. In a gel filtration approach, LETM1 was similarly found in a higher MW complex of a compatible ∼540 kDa size (20). Silencing or overexpression of LETM1 did not change the occurrence of the different complexes, suggesting that LETM1 does not have an essential scaffolding role. In other words, either the complexes are composed solely by

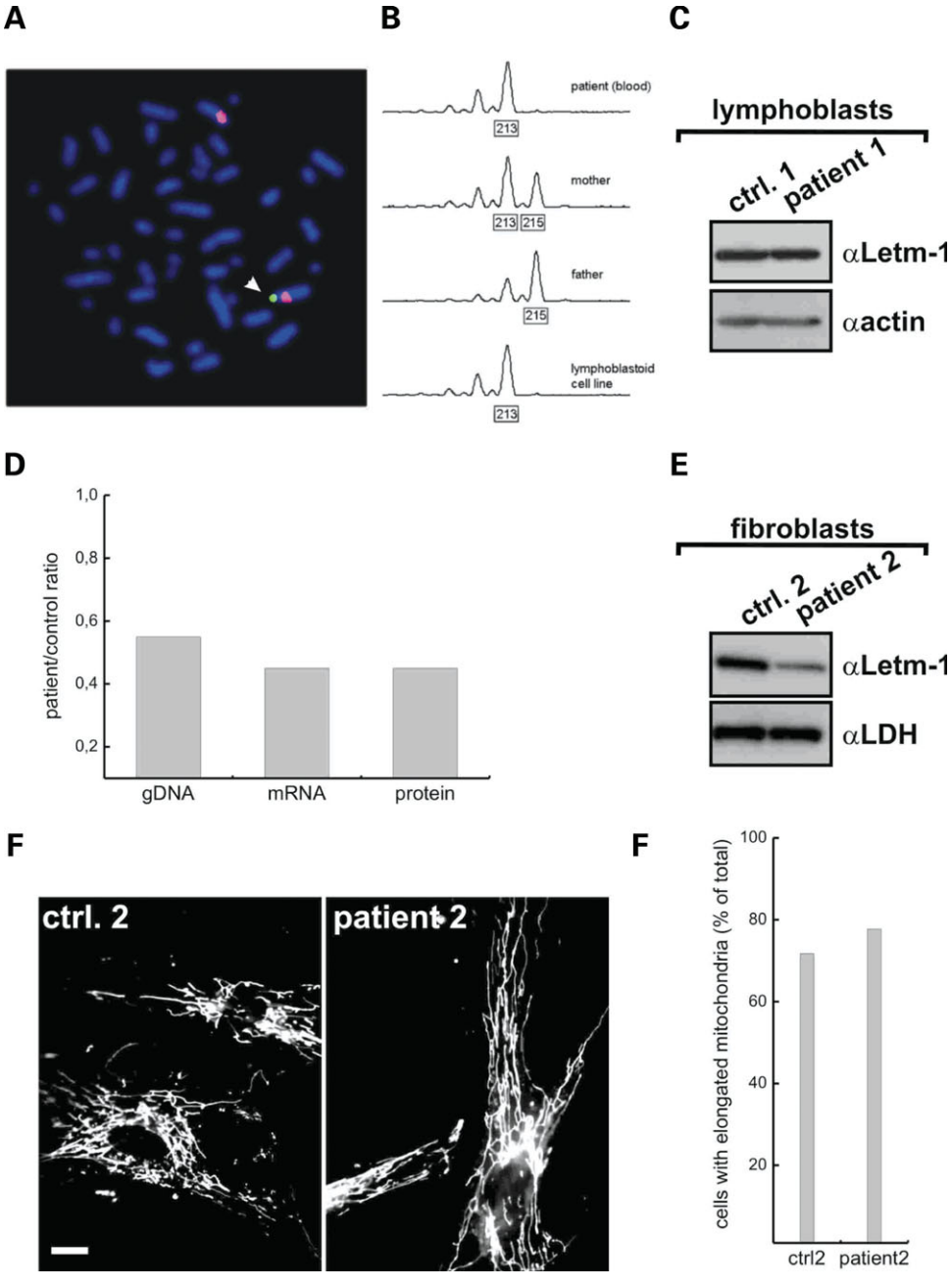

Figure 6. LETM1 levels and mitochondrial morphology in cells from two WHS patients. (**A**) FISH analysis with cosmid LA04NC01-75b9 (green) and a chromosome 4 specific centromere probe (red) indicating deletion of *LETM1* on one chromosome (arrow). (**B**) Analysis of microsatellite marker MS-27h9, representing a dinucleotide polymorphism 182 kb centromeric to *LETM1*. The patient (DNA from blood sample as well as the lymphoblastoid cell line) inherited a 213 bp allel from the heterozygous mother (215 and 213 bp alleles), but not the 215 bp allele from the homozygous father. (**C**) Levels of LETM1 in control (ctrl.) and WHS patient lymphoblasts. Cells were lysed and equal amounts of protein (10 μg) were separated by SDS–PAGE and immunoblotted using the indicated antibodies. Blots are representative of six different experiments. (**D**) Patient:control ratio of *LETM1* in genomic DNA (gDNA), messenger RNA (mRNA) and of LETM1 protein (determined on the same sample by densitometry following immunoblotting). *LETM1* levels in gDNA and mRNA were measured by RT-PCR as described (**E**) Levels of LETM1 in control (ctrl. 2) and WHS patient (patient 2) fibroblasts. Cells were lysed and equal amounts of protein (10 μg) were separated by SDS–PAGE and immunoblotted using the indicated antibodies. Blots correspond to the sample analyzed in panel (D). (**F**) Mitochondrial morphology in control (ctrl. 2) and WHS patient (patient 2) fibroblasts. Cells were loaded for 30 min with 20 nM TMRM and representative epifluorescence images were acquired as described in Materials and Methods. Bar, 15 μm. (**G**) Quantitative analysis of mitochondrial morphology control (ctrl. 2) and WHS patient (patient 2) fibroblasts. Experiments were as in (F). Total cell number was 106 (ctrl. 2) and 110 (patient 2) in two independent experiments.

LETM1 molecules that homo-oligomerize according to their ability to self interact (20), or their structural integrity does not depend on the presence of LETM1.

The loss of LETM1 results in striking morphological abnormalities of mitochondria, which appear fragmented and clustered in the perinuclear region. This was similar to the

morphologies observed following overexpression of pro-fission molecules like Fis1 or ablation of pro-fusion ones like Opa1 (22,23). Nevertheless, mitochondrial morphology was not recovered by ablation or inhibition of the fission pathway. This suggests that fragmentation of mitochondria lacking LETM1 does not require activation of the Drp1-dependent fission pathway, at a major variance from what observed in the case of overexpression of other pro-fission proteins (24) or ablation of pro-fusion ones (25). The unusual independence from Drp1 could imply that the fragmentation caused by silencing of *LETM1* is not caused by an unbalance in the fusion–fission equilibrium; rather, it could represent the morphological counterpart of a mitochondrial sufferance that follows the inhibition of a crucial function of ion homeostasis or protein export into the inner membrane. In particular, mitochondria with lower levels of LETM1 rounded up and seemed to be enlarged. The 'ring' shape observed following LETM1 overexpression could be the result of matrix shrinkage, followed by network fragmentation and ring-like closure of mitochondria to obtain a more stable structure. Alternatively, this morphology could represent a non-specific mitochondrial damage, supported by the retrieval in these mitochondria of proteolysis products of LETM1 that lie outside the complexes containing the native protein. On the other hand, the fragmented and enlarged morphology of mitochondria with less LETM1 was complemented by the antibiotic nigericin, which exchanges K^+ with protons and therefore can be considered a pharmacological K^+/H^+ antiporter. This evidence strongly supports a role for LETM1, like its yeast orthologue Mdm38p, in the regulation of the extrusion of K^+ from the mitochondrial matrix. If LETM1 is the antiporter, or it is one of its regulators, remain an open question. In principle, other ion exchangers display a much more complex structure, with 12 transmembrane helices. Conversely, the EF hands identified in LETM1 display a low affinity for divalent ions, suggesting that they could bind matricial Mg^{2+} rather than Ca^{2+} (6). It should be kept in mind that the K^+/H^+ antiporter is indeed directly regulated by matricial Mg^{2+} (36); and that the MW weight of LETM1 is compatible with the $\sim$80 kDa protein identified by Garlid and colleagues (37) as the putative antiporter. On the other hand, one would expect that mitochondria with impaired K^+ extrusion and deranged volume homeostasis would be dysfunctional, but all our attempts to unveil a dysfunction in mitochondria where *LETM1* was silenced failed. Respiration, membrane potential, steady-state levels of nuclear encoded, exported subunits of the respiratory chain were all apparently normal. Furthermore, we could not detect an interaction between LETM1 and ribosomal protein of mitochondria (not shown), as proposed for its yeast orthologue Mdm38p (19). We cannot exclude that the residual 40% of LETM1 protein can maintain mitochondrial function or protein export. In this case, mitochondrial shape would represent the most sensible indicator of mitochondrial damage. In conclusion, our morphological analysis supports a role for LETM1 in ion and therefore volume homeostasis across the inner membrane.

Ablation of Letm1 in *C. elegans* is lethal and yeast strains lacking Mdm38p display growth defects on non-fermentable carbon sources. Similarly, we could not generate clones where *LETM1* was stably ablated by RNAi (not shown) and transient down-regulation of the levels of the protein was associated with spontaneous death. The features of this death were indeed more 'necrotic', with permeabilization of the plasma membrane to PI. Interestingly, caspases were not activated and their inhibition did not counteract death; moreover, Bcl-2, which keeps in check release of cytochrome *c* from mitochondria (38) and is a primary inhibitor of most intrinsic apoptotic stimuli (39), did not prevent death that follows reduction in LETM1 levels. Cells can die by the so-called 'caspase-independent' mode of apoptosis, relying on the release of factors like AIF, Omi, EndoG that directly act at the nuclear level to exert DNA degradation. However, their release from mitochondria is similarly controlled by Bcl-2 (40). In this respect, it is unlikely that lack of LETM1 primes 'caspase-independent' apoptosis, since it is not blocked by Bcl-2. Failure of inhibition by Bcl-2 apparently rules out also the possibility that lack of LETM1 results in autophagy, also blocked by enforced expression of Bcl-2 (41).

We established two cell models, a transformed lymphoblast cell line and a primary fibroblast culture, derived from two different full clinical picture WHS patients. Genetic analysis revealed that in both samples one allele of *LETM1* was lacking, but in the case of the lymphoblasts the levels of the protein seemed unchanged as compared to an age- and sex-matched control lymphoblast line. A similar situation was observed by van der Bliek and colleagues in fibroblasts (20), opening the possibility that *LETM1* displays a monoallelic expression, and that its protein levels are therefore unaffected by the loss of a single allele. Although we have not investigated mono- or biallelic expression in humans, we could at least demonstrate biallelic expression of *Letm1* in various murine tissues (not shown), which strongly indicates a similar situation in human. We deepened our analysis by generating a second cellular model from a different WHS patient. In the case of this primary fibroblast culture, we could demonstrate a $\sim$50% reduction in the levels of *LETM1* gene, messenger and LETM1 protein. It should be stressed that the reduction in LETM1 protein levels appeared somehow variable. Thus, the results in lymphoblasts could be a consequence of the transformed nature of this cell line, or be ascribed to an even higher variability in this protein levels reduction. Irrespective of this, mitochondrial morphology in WHS fibroblasts was unexpectedly superimposable to that observed in the controls. This result opens the possibility that the striking phenotype of fragmentation of the organelle observed in HeLa cells depended on the efficient down-regulation observed following RNAi. In other words, there is a strict threshold of LETM1 levels that must be crossed in other to obtain a clear phenotype. Alternatively, there could be a yet uncharacterized effect of the other genes deleted in WHS (on mitochondrial morphology, which could compensate the fragmentation caused by the monoallelic loss of *LETM1*.

Whether LETM1 is still a good candidate for the pathogenesis of seizures in WHS remains an open question. So far, three different cell models from WHS patients [two described here and one in (20)] failed to display the same mitochondrial alterations observed by deleting the gene in yeast and *C. elegans*, or by down-regulating it in cultured mammalian cells. Nevertheless, no studies have been so far performed in neurons, which are known to critically depend on

mitochondrial function and dynamics (42,43). In conclusion, it appears that function of LETM1 should be investigated in neurons, and that a mouse model of *Letm1* ablation is required to understand the role of this protein in the CNS and in the pathogenesis of seizures.

MATERIALS AND METHODS

SDS–PAGE, western blotting and antibodies

Proteins were separated by 4–12% Tris-MOPS SDS–PAGE (NuPage, Invitrogen) transferred onto PVDF membranes (Millipore) and probed using the indicated antibodies. The following antibodies were used: monoclonal anti-LETM1 (1:500, Abnova, Taipei, Taiwan); polyclonal anti-LETM1 [1:1000 (6)]; polyclonal anti-Tom20 (1:2000, Santa Cruz Biotechnology), anti-Serca2 (1:500, Santa Cruz Biotechnology) antiGrp75 (mtHsp70, 1:500, Santa Cruz Biotechnology); monoclonal anti-Opa1 (1:500, BD Biosciences, Lexington, KY); monoclonal anti-cytochrome *c* (1:500, BD Biosciences); polyclonal anti-MnSOD (1:3000, Nventa Biopharmaceuticals, San Diego, CA); monoclonal anti-PARP (1:5000, Cell Signaling Technology, Danvers, MA); polyclonal anti-MnSOD (1:2000, Invitrogen, Novato, CA); polyclonal anti-LDH (1:1000, Rockland, Gilbertsville, PA) and polyclonal anti-Mfn2 (44) (1:200, a kind gift from Dr M. Rojo). Purified antibodies raised against isolated OXPHOS complexes were a kind gift by Dr L. Vergani and included: anti-complex I (polyclonal anti 51 kDa subunit); anti-complex II (polyclonal anti 70 kDa subunit); complex III (polyclonal anti bc1 (45)) and anti-ATPase (polyclonal anti-αβ subunit). All anti OXPHOS antibodies were used at a final dilution of 1:1000. Isotype matched, horse-radish peroxidase-conjugated secondary antibodies (Sigma) were used followed by detection by chemiluminescence (Amersham).

Molecular biology

Two siRNA against *LETM1* were synthesized from the following sequences 5′-GGA ACU GCC UGA AUG UUC Ctt-3′, and 5′-CAG AGA CUU CCA UAA UCA Att-3′ and were used in combination at a final concentration of 100 nM each. The scrambled control siRNA (5′-GUA GCA CGC GUA ACU GUC Utt-3′) was used at the same final concentration. All siRNA were obtained from Ambion (Huntington, UK).

The cDNA of LETM1 was cloned in the *Eco*RI, *Xho*I sites of pcDNA3 (Invitrogen, Carlsbad, CA). Constructs were confirmed by sequencing. Mitochondrially targeted red fluorescent protein (mtRFP) corresponded to pDsRed2-Mito and was from Clonetech (Mountain View, CA).

Quantitative analysis of *LETM1* gene dosage and expression

Genomic DNA and total RNA from cultured fibroblasts were extracted using standard methods and prepared for subsequent analysis. mRNA was retrotranscribed using Superscript II RT–PCR Kit and random hexameres (Invitrogen). Real-time quantitative PCR was performed using Power SYBR Green PCR Master Mix and a 7900 Genetic Analyzer (Applied Biosystems). Reaction conditions were standard (95°C 15 s, 60°C 30 s; 40 cycles). Oligonucleotides used in the reaction were 5′-GGGAGCGCAGGCAGTTT-3′ and 5′-ACAGCAACAGGCAGCAGAAA-3′ for genomic DNA and 5′-GGGCACAGGCGTGAGATG-3′ and 5′- CTGCATTCCAACTGCTC AGACT-3′ for mRNA. Results were normalized to the albumin gene to evaluate genomic DNA copy number, and to GUS for mRNA expression. Data were analyzed using the Delta/Delta CT method as previously reported (46).

Cell culture and transfection

Human primary fibroblasts were obtained at the Department of Pediatrics, University of Padova, from a 20 years old female patient during elective spinal surgery, with informed consent of the parents, her legal representatives. The diagnosis had been previously established by chromosomal analysis and 4p16 FISH. Control fibroblasts were obtained from an age- and sex-matched healthy donor by cutaneous biopsy.

Cells were cultured in Dulbecco's Modified Eagle's Medium (DMEM) (Gibco) supplemented with 10% fetal bovine serum (Gibco), 50 U/ml Penicillin, 50 μg/ml Streptomycin, 100 μM non-essential aminoacids (MEM, Gibco/Invitrogen) and 2 mM glutamine (Gibco).

A lymphoblastoid cell line was established from a female WHS patient at the Institute of Human Genetics, University Hospital Erlangen, with informed consent of the patient's legal representative. Deletion was verified by FISH as well as by microsatellite analysis. Microsatellite analysis was performed using fluorescently labelled primers 27h9-F: 5′-GAGACCAGCTTAGGTAACG-3′ and 27h9-R: 5′-GGCTG TGGTGAGTTGTTTG-3′ to amplify a polymorphic region at cosmid LA04NC01-27H9 (Acc. Z49237) (at ∼2.022 Mb). PCR products were electrophoresed using an ABI3100 sequencer and results were analyzed using genescan and genotyper software (Applied Biosystems).

HeLa cells stably expressing Bcl-2 ($HeLa^{Bcl\text{-}2}$) and their respective control carrying the empty vector ($HeLa^{neo}$) (47) were a kind gift from P. Bernardi (University of Padova). HeLa cells stably expressing mtRFP were generated by selection with the antibiotic G418 (500 μg/ml) followed by clonal selection by limiting dilution. Homogeneous expression of mtRFP was confirmed by flow cytometry and cells were grown in DMEM supplemented as above, plus G418 (500 μg/ml). Transfection of HeLa cells with siRNA and plasmid DNA was performed with Lipofectamine 2000 (Invitrogen) according to the manufacturer's protocol.

Mitochondrial isolation and subfractionation

Mitochondrial isolation from 10^9 HeLa cells was performed by standard differential centrifugation as previously described (48). To isolate the light membrane and the cytosolic fraction, the post-mitochondrial supernatant was spun twice for 30 min at 100 000*g* to separate pellet (light membranes) and supernatant (cytosol). Protein in separated fractions was determined by a BCA protein assay (Pierce).

Submitochondrial fractionation was performed according to Sottocasa *et al*. (49). Briefly, 50 mg of mitochondria were resuspended in 10 ml of 10 mM KH_2PO_4 using a Teflon

pestle. Mitochondria were left on ice for 5 min and spun at 8000*g* for 10 min. The supernatant was recovered and the pellet resuspended in 125 mM KCl, 10 mM Tris-MOPS pH 7.4, centrifuged again and the former with the latter supernatant constituted the IMS fraction. The pellet was resuspended in 10 ml of 10 mM KH_2PO_4 and 3.5 ml of a solution containing 1.8 M sucrose, 2 mM ATP, 2 mM $MgSO_4$ were added. After 5 min the sample was sonicated at 4 W for 20 min, laid on the top of 15 ml of a solution containing 1.18 M sucrose and spun for 2 h at 90 000*g*. After the centrifugation, an upper soluble clear layer corresponding to the matrix (M) fraction, a yellow interphase corresponding to the outer membrane (OM) and a brown pellet corresponding to the IM were collected.

Protease-accessibility assay

Mitochondria (0.1 mg/ml) resuspended in isolation buffer (IB, 0.2 M sucrose, 10 mM Tris-Mops pH 7.4, 0.1 mM EGTA-Tris) were treated with 100 μg/ml PK at 4°C for 30 min. Where indicated, hypotonic rupture of the OM was achieved by diluting the mitochondrial suspension 1:40 in 2 mM HEPES/KOH pH 7.4; Triton X-100 was added where indicated at a final concentration of 0.3% (V/V). PK was inactivated by incubation with 1 mM PMSF at 4°C for 5 min. The resulting samples were precipitated with 10% trichloroacetic acid (TCA), spun at 4°C, 18 000*g* for 30 min, and the pellet was washed with cold acetone, resuspended in 100 μl of NuPAGE loading buffer (Invitrogen) and a tenth (10 μg) was loaded on a gel.

Crosslinking and blue native gel electrophoresis

For crosslinking, mitochondria (0.1 mg/ml) were incubated in 20 mM HEPES/KOH pH 7.4, 125 mM KCl, 1 mM KPI and treated with 500 μM BMH for 30 min at room temperature, or with 500 μM DSS (Pierce) at 4°C for 30 min. Samples were TCA-precipitated as described above and 30 μg of protein was separated by SDS–PAGE and immunoblotted.

The blue native gel electrophoresis was performed using the NativePAGE™ Novex® Bis-TrisGel System (Invitrogen) according to manufacturer's protocol. The first dimension was separated on a 4–16% gradient NativePAGE Gel. Samples from isolated mitochondria were prepared with the NativePAGE™ Sample Prep Kit following the instructions of the manufacturer. For solubilization, DDM was used in two different final concentrations of 1.2 and 2.5% (w/V) and 50 μg of solubilized mitochondrial protein were separated. For the second dimension, a 4–12% Bis-Tris NuPAGE-Gel was used in the SDS–PAGE.

Imaging

For real-time imaging, cells seeded onto 24-mm round glass coverslips were transfected as indicated and after 48 h loaded with 10 nM TMRM (Molecular Probes) in the presence of 2 mg/ml cyclosporine H (Sigma), a P-glycoprotein inhibitor (30 min at 37°C). Subsequently cells were placed on the stage of an Olympus IX81 inverted microscope equipped with a CellR Imaging system. Sequential images of TMRM fluorescence were acquired every 60 s using exposure times of 30 ms with a 40×, 1.4 NA Plan Apo objective (Olympus), a 525 ± 20 excitation filter and an emission 570 LP filter. Images were stored for subsequent analysis, background subtraction and normalization which was performed exactly as described previously (13).

For confocal imaging of the mitochondrial network, 6×0^4 HeLa cells stably expressing mtRFP were seeded onto 24 mM-round glass coverslips and transfected as indicated. After 24–48 h cells were incubated in Hank's Balanced Salt Solution (HBSS) supplemented with 10 mM HEPES and coverslips were placed on the stage of a Nikon Eclipse TE300 inverted microscope equipped with a spinning-disk Perkin Elmer Ultraview LCI confocal system and a Orca ER 12-bit CCD camera (Hamamatsu). Cells were excited using the 543 nm line of the He-Ne laser (Perkin Elmer) with exposure times of 50 ms using a 60 × 1.4 NA Plan Apo objective (Nikon).

For epifluorescence imaging of the mitochondrial network, 6×0^4 HeLa cells stably expressing mtRFP were seeded onto 24 mM-round glass coverslips and transfected as indicated. After 24–48 h, cells were incubated in HBSS supplemented with 10 mM HEPES and coverslips were placed on the stage of a Olympus IX81 inverted microscope equipped with a CellR imaging system (Olympus). Cells were excited using the 525 ± 20 excitation filter and emitted light was collected using a 570 LP filter with exposure times of 50 ms using a 40 × 1.4 NA Plan Apo objective (Olympus). Where indicated, images were deconvolved using the convolution filter of the program ImageJ (NIH). Morphometric analysis was performed as described previously (23).

Flow cytometry

For evaluation of membrane potential, HeLa cells were grown in 6-well plates, transfected as indicated and after 48 h harvested. Cells were washed with PBS, resuspended in HBSS supplemented with 10 mM HEPES and loaded with 10 nM TMRM (Molecular Probes) in the presence of 2 mg/ml cyclosporine H, a P-glycoprotein inhibitor and 50 mM KCl (30 min at 37°C). Cells were then analyzed by flow cytometry using with a FACSCalibur cytometer (Becton-Dickinson).

For evaluation of apoptosis, 5×10^5 HeLa, $HeLa^{neo}$ or $HeLa^{Bcl2}$ cells were grown in 6-well plates and transfected with siRNA as indicated. After 24–48 h, cells were harvested and stained with PI and Annexin-V-FLUOS (Roche) according to manufacturer's protocol. Viability was measured by flow cytometry as the percentage Annexin-V, PI negative cells.

ACKNOWLEDGEMENTS

We wish to thank PD Dr Anita Rauch (Erlangen) for help with the patient and the fluorescence *in situ* hybridization.

Conflict of Interest statement. None declared.

FUNDING

L.S. is a Senior Telethon Scientist of the Dulbecco-Telethon Institute and this research was supported by Telethon Italy,

AIRC Italy, Compagnia di San Paolo, UMDF. K.S.D. is supported by a Long-Term Fellowship of the Federation of European Biochemical Societies (FEBS).

REFERENCES

1. Bergemann, A.D., Cole, F. and Hirschhorn, K. (2005) The etiology of Wolf–Hirschhorn syndrome. *Trends Genet.*, **21**, 188–195.
2. Zollino, M., Lecce, R., Fischetto, R., Murdolo, M., Faravelli, F., Selicorni, A., Butte, C., Memo, L., Capovilla, G. and Neri, G. (2003) Mapping the Wolf–Hirschhorn syndrome phenotype outside the currently accepted WHS critical region and defining a new critical region, WHSCR-2. *Am. J. Hum. Genet.*, **72**, 590–597.
3. Wright, T.J., Ricke, D.O., Denison, K., Abmayr, S., Cotter, P.D., Hirschhorn, K., Keinanen, M., McDonald-McGinn, D., Somer, M., Spinner, N. *et al.* (1997) A transcript map of the newly defined 165 kb Wolf–Hirschhorn syndrome critical region. *Hum. Mol. Genet.*, **6**, 317–324.
4. Wright, T.J., Costa, J.L., Naranjo, C., Francis-West, P. and Altherr, M.R. (1999) Comparative analysis of a novel gene from the Wolf–Hirschhorn/Pitt-Rogers-Danks syndrome critical region. *Genomics*, **59**, 203–212.
5. Buckle, V.J., Fujita, N., Ryder-Cook, A.S., Derry, J.M.J., Barnard, P.J., Lebo, R.V., Schofield, R., Seeburg, P.H., Bateson, A.N., Darlison, M.G. and Barnard, E.A. (1989) Chromosomal localization of GABAA receptor subunit genes: relationship to human genetic disease. *Neuron*, **3**, 647–654.
6. Endele, S., Fuhry, M., Pak, S.J., Zabel, B.U. and Winterpacht, A. (1999) LETM1, a novel gene encoding a putative EF-hand Ca(2+)-binding protein, flanks the Wolf–Hirschhorn syndrome (WHS) critical region and is deleted in most WHS patients. *Genomics*, **60**, 218–225.
7. Schlickum, S., Moghekar, A., Simpson, J.C., Steglich, C., O'Brien, R.J., Winterpacht, A. and Endele, S.U. (2004) LETM1, a gene deleted in Wolf–Hirschhorn syndrome, encodes an evolutionarily conserved mitochondrial protein. *Genomics*, **83**, 254–261.
8. Jouaville, L.S., Ichas, F., Holmuhamedov, E.L., Camacho, P. and Lechleiter, J.D. (1995) Synchronization of calcium waves by mitochondrial substrates in *Xenopus laevis* oocytes. *Nature*, **377**, 438–441.
9. Wang, X. (2001) The expanding role of mitochondria in apoptosis. *Genes Dev.*, **15**, 2922–2933.
10. Frank, S., Gaume, B., Bergmann-Leitner, E.S., Leitner, W.W., Robert, E.G., Catez, F., Smith, C.L. and Youle, R.J. (2001) The role of dynamin-related protein 1, a mediator of mitochondrial fission, in apoptosis. *Dev. Cell*, **1**, 515–525.
11. Scorrano, L., Ashiya, M., Buttle, K., Weiler, S., Oakes, S.A., Mannella, C.A. and Korsmeyer, S.J. (2002) A Distinct pathway remodels mitochondrial cristae and mobilizes cytochrome c during apoptosis. *Dev. Cell*, **2**, 55–67.
12. Cipolat, S., Rudka, T., Hartmann, D., Costa, V., Serneels, L., Craessaerts, K., Metzger, K., Frezza, C., Annaert, W., D'Adamio, L. *et al.* (2006) Mitochondrial rhomboid parl regulates cytochrome c release during apoptosis via opa1-dependent cristae remodeling. *Cell*, **126**, 163–175.
13. Frezza, C., Cipolat, S., Martins, d.B., Micaroni, M., Beznoussenko, G.V., Rudka, T., Bartoli, D., Polishuck, R.S., Danial, N.N., De Strooper, B. and Scorrano, L. (2006) OPA1 controls apoptotic cristae remodeling independently from mitochondrial fusion. *Cell*, **126**, 177–189.
14. DiMauro, S., Kulikova, R., Tanji, K., Bonilla, E. and Hirano, M. (1999) Mitochondrial genes for generalized epilepsies. *Adv. Neurol.*, **79**, 411–419.
15. Wasterlain, C.G., Niquet, J., Thompson, K.W., Baldwin, R., Liu, H., Sankar, R., Mazarati, A.M., Naylor, D., Katsumori, H., Suchomelova, L. and Shirasaka, Y. (2002) Seizure-induced neuronal death in the immature brain. *Prog. Brain Res.*, **135**, 335–353.
16. Dimmer, K.S., Fritz, S., Fuchs, F., Messerschmitt, M., Weinbach, N., Neupert, W. and Westermann, B. (2002) Genetic basis of mitochondrial function and morphology in *Saccharomyces cerevisiae*. *Mol. Biol. Cell*, **13**, 847–853.
17. Nowikovsky, K., Froschauer, E.M., Zsurka, G., Samaj, J., Reipert, S., Kolisek, M., Wiesenberger, G. and Schweyen, R.J. (2004) The LETM1/YOL027 gene family encodes a factor of the mitochondrial K+ homeostasis with a potential role in the Wolf–Hirschhorn syndrome. *J. Biol. Chem.*, **279**, 30307–30315.
18. Bernardi, P. (1999) Mitochondrial transport of cations: channels, exchangers and permeability transition. *Physiol. Rev.*, **79**, 1127–1155.
19. Frazier, A.E., Taylor, R.D., Mick, D.U., Warscheid, B., Stoepel, N., Meyer, H.E., Ryan, M.T., Guiard, B. and Rehling, P. (2006) Mdm38 interacts with ribosomes and is a component of the mitochondrial protein export machinery. *J. Cell Biol.*, **172**, 553–564.
20. Hasegawa, A. and van der Bliek, A.M. (2007) Inverse correlation between expression of the Wolfs Hirschhorn candidate gene Letm1 and mitochondrial volume in *C. elegans* and in mammalian cells. *Hum. Mol. Genet.*, **16**, 2061–2071.
21. Meier, S., Neupert, W. and Herrmann, J.M. (2005) Proline residues of transmembrane domains determine the sorting of inner membrane proteins in mitochondria. *J. Cell Biol.*, **170**, 881–888.
22. Alirol, E., James, D., Huber, D., Marchetto, A., Vergani, L., Martinou, J.C. and Scorrano, L. (2006) The mitochondrial fission protein hFis1 requires the endoplasmic reticulum gateway to induce apoptosis. *Mol. Biol. Cell*, **17**, 4593–4605.
23. Cipolat, S., de Brito, O.M., Dal Zilio, B. and Scorrano, L. (2004) OPA1 requires mitofusin 1 to promote mitochondrial fusion. *Proc. Natl. Acad. Sci. USA*, **101**, 15927–15932.
24. James, D.I., Parone, P.A., Mattenberger, Y. and Martinou, J.C. (2003) hFis1, a novel component of the mammalian mitochondrial fission machinery. *J. Biol. Chem.*, **278**, 36373–36379.
25. Sesaki, H., Southard, S.M., Yaffe, M.P. and Jensen, R.E. (2003) Mgm1p, a dynamin-related GTPase, is essential for fusion of the mitochondrial outer membrane. *Mol. Biol. Cell*, **14**, 2342–2356.
26. Scorrano, L., Petronilli, V. and Bernardi, P. (1997) On the voltage dependence of the mitochondrial permeability transition pore. A critical appraisal. *J. Biol. Chem.*, **272**, 12295–12299.
27. Kucejova, B., Kucej, M., Petrezselyova, S., Abelovska, L. and Tomaska, L. (2005) A Screen for Nigericin-resistant yeast mutants revealed genes controlling mitochondrial volume and mitochondrial cation homeostasis. *Genetics*, **171**, 517–526.
28. Irwin, W.A., Bergamin, N., Sabatelli, P., Reggiani, C., Megighian, A., Merlini, L., Braghetta, P., Columbaro, M., Volpin, D., Bressan, G.M. *et al.* (2003) Mitochondrial dysfunction and apoptosis in myopathic mice with collagen VI deficiency. *Nat. Genet.*, **35**, 367–371.
29. Danial, N.N. and Korsmeyer, S.J. (2004) Cell death: critical control points. *Cell*, **116**, 205–219.
30. Wong, E.D., Wagner, J.A., Gorsich, S.W., McCaffery, J.M., Shaw, J.M. and Nunnari, J. (2000) The dynamin-related GTPase, Mgm1p, is an intermembrane space protein required for maintenance of fusion competent mitochondria. *J. Cell Biol.*, **151**, 341–352.
31. Frezza, C., Cipolat, S., Martins, d.B., Micaroni, M., Beznoussenko, G.V., Rudka, T., Bartoli, D., Polishuck, R.S., Danial, N.N., De Strooper, B. and Scorrano, L. (2006) OPA1 controls apoptotic cristae remodeling independently from mitochondrial fusion. *Cell*, **126**, 177–189.
32. Dimmer, K.S., Jakobs, S., Vogel, F., Altmann, K. and Westermann, B. (2005) Mdm31 and Mdm32 are inner membrane proteins required for maintenance of mitochondrial shape and stability of mitochondrial DNA nucleoids in yeast. *J. Cell Biol.*, **168**, 103–115.
33. Messerschmitt, M., Jakobs, S., Vogel, F., Fritz, S., Dimmer, K.S., Neupert, W. and Westermann, B. (2003) The inner membrane protein Mdm33 controls mitochondrial morphology in yeast. *J. Cell Biol.*, **160**, 553–564.
34. Scorrano, L. (2005) Proteins that fuse and fragment mitochondria in apoptosis: con-fissing a deadly con-fusion? *J. Bioenerg. Biomembr.*, **37**, 165–170.
35. Dimmer, K.S. and Scorrano, L. (2006) (De)constructing mitochondria: what for? *Physiology (Bethesda)*, **21**, 233–241.
36. Nakashima, R.A., Dordick, R.S. and Garlid, K.D. (1982) On the relative roles of Ca2+ and Mg2+ in regulating the endogenous K+/H+ exchanger of rat liver mitochondria. *J. Biol. Chem.*, **257**, 12540–12545.
37. Martin, W.H., Beavis, A.D. and Garlid, K.D. (1984) Identification of an 82,000-dalton protein responsible for K+/H+ antiport in rat liver mitochondria. *J. Biol. Chem.*, **259**, 2062–2065.
38. Kluck, R.M., Bossy-Wetzel, E., Green, D.R. and Newmeyer, D.D. (1997) The release of cytochrome c from mitochondria: a primary site for Bcl-2 regulation of apoptosis. *Science*, **275**, 1132–1136.

39. Hockenbery, D., Nunez, G., Milliman, C., Schreiber, R.D. and Korsmeyer, S.J. (1990) Bcl-2 is an inner mitochondrial membrane protein that blocks programmed cell death. *Nature*, **348**, 334–336.
40. Donovan, M. and Cotter, T.G. (2004) Control of mitochondrial integrity by Bcl-2 family members and caspase-independent cell death. *Biochim. Biophys. Acta Mol. Cell Res.*, **1644**, 133–147.
41. Pattingre, S., Tassa, A., Qu, X., Garuti, R., Liang, X.H., Mizushima, N., Packer, M., Schneider, M.D. and Levine, B. (2005) Bcl-2 antiapoptotic proteins inhibit beclin 1-dependent autophagy. *Cell*, **122**, 927–939.
42. Kann, O. and Kovacs, R. (2007) Mitochondria and neuronal activity. *Am. J. Physiol. Cell Physiol.*, **292**, C641–C657.
43. Li, Z., Okamoto, K., Hayashi, Y. and Sheng, M. (2004) The importance of dendritic mitochondria in the morphogenesis and plasticity of spines and synapses. *Cell*, **119**, 873–887.
44. Rojo, M., Legros, F., Chateau, D. and Lombes, A. (2002) Membrane topology and mitochondrial targeting of mitofusins, ubiquitous mammalian homologs of the transmembrane GTPase Fzo. *J. Cell Sci.*, **115**, 1663–1674.
45. Petronilli, V., Penzo, D., Scorrano, L., Bernardi, P. and Di Lisa, F. (2001) The mitochondrial permeability transition, release of cytochrome c and cell death. Correlation with the duration of pore openings in situ. *J. Biol. Chem.*, **276**, 12030–12034.
46. Casarin, A., Martella, M., Polli, R., Leonardi, E., Anesi, L. and Murgia, A. (2006) Molecular characterization of large deletions in the von Hippel-Lindau (VHL) gene by quantitative real-time PCR: the hypothesis of an alu-mediated mechanism underlying VHL gene rearrangements. *Mol. Diagn. Ther.*, **10**, 243–249.
47. Milanesi, E., Costantini, P., Gambalunga, A., Colonna, R., Petronilli, V., Cabrelle, A., Semenzato, G., Cesura, A.M., Pinard, E. and Bernardi, P. (2006) The mitochondrial effects of small organic ligands of BCL-2: sensitization of BCL-2-overexpressing cells to apoptosis by a pyrimidine-2,4,6-trione derivative. *J. Biol Chem.*, **281**, 10066–10072.
48. Frezza, C., Cipolat, S. and Scorrano, L. (2007) Organelle isolation: functional mitochondria from mouse liver, muscle and cultured fibroblasts. *Nat. Protoc.*, **2**, 287–295.
49. Sottocasa, G.L., Kuylenstierna, B., Ernster, L. and Bergstrand, A. (1967) An electron-transport system associated with the outer membrane of liver mitochondria. A biochemical and morphological study. *J. Cell Biol.*, **32**, 415–438.